CrystEngComm

Accepted Manuscript

ROYAL SOCIETY OF CHEMISTRY

www.rsc.org/crystengcomm

CrystEngComm

ARTICLE

Study of temperature and ligand flexibility effects on coordination polymers formation from cyclobutanetetracarboxylic acid

Received 00th March 2015,
Accepted 00th March 2015

DOI: 10.1039/x0xx00000x

www.rsc.org/

Lizaira Bello,[a] Marilyn E. Quintero,[a,b] Asiloé J. Mora,[b] Teresa González,[a] Ana M. Escalona,[a] Rafael Añez,[c] Edward E. Ávila,[*a] and Alexander Briceño[*a]

Three new coordination polymers based on the combination of *rctt*-1,2,3,4-cyclobutanetretracarboxylic acid (***rctt*-H$_4$Cbtc**) and trans-1,2-bis(4-pyridyl)ethane (4,4'-**bpe**) and Zn and Ni metal centers were synthesized under hydrothermal conditions and structurally characterized either by X-ray Single Crystal or Powder Diffraction: [Zn_2(4,4'-**bpe**)(***rctt*-Cbtc**)$(OH_2)]_n \cdot 4H_2O$ (**1**), [Zn(4,4'-**bpe**)$_{0.5}$(***rctt*-Cbtc**)$_{0.5}(OH_2)]_n$ (**2**) and [Ni_2(4,4'-**bpe**)$_2$(***rctt*-Cbtc**)$(OH_2)_6$] (**3**). The crystal structure of **1** formed a 3-D coordination polymer. A similar building unit is found in **2** but forming part of a polymeric 2-D array, where the bipyridine displays a gauche conformation in contrast to the anti conformation found for **1**. In **3**, the change of Zn by Ni as a node produces a novel supramolecular array based on an 1-D coordination polymer, which is constructed from chains bearing 4,4'-**bpe** in an *anti* configuration. A sequential hydrothermal transformation was observed between **1** and **2** in the range of 80 and 120 °C, respectively. An increase of time or temperature of reaction favored the formation of **2** below 140 °C. Solid phases **1** and **2** are metastable above 140 °C. A novel unidentified phase is observed at 180 °C, starting from the same chemical precursors in a similar molar ratio. DFT calculations corroborate the experimental observations; compound **2** is a few more stable than **1**. The energy lost when water leaves the Zn atom is partially compensated by the O atom of the ***rctt*-Cbtc** ligand and could induce the formation of compound **2**.

Introduction

The study of self-assembly of coordination polymers containing transition metals and mixed organic linkers has been of great interest to many researchers in recent years, especially in applications such as gas adsorption,[1-4] catalysis,[5-7] proton conductivity,[8-10] drug release,[11-12] among others. In particular, coordination polymers that exhibit dynamic behavior capable to undergo reversible structural transformations of the type crystal-to-crystal or crystal-amorphous triggered by external stimuli represent a fascinating property of such materials (e.g., adsorption/desorption of guest molecules, ion to ligand exchange, mechanical, thermal and photochemical perturbation).[13] Synthesis of such materials depend on several factors, among which the coordination spheres of the metal centers, using either primary or secondary building blocks, are key elements. Thus, the possibility of combining more than one building block unit provides a simple route to design novel modular supramolecular architectures, making possible the fine-tuning of physicochemical properties from the adequate choice of organic components with contrasting properties, e.g. rigidity/flexibility, bent/lineal connection points, hydrophobicity/hydrofilicity of the supramolecular periphery, etc. Such structural properties in combination with metal centers allow to obtain unique supramolecular networks with unusual cooperative behavior, bearing tunable rigid and flexible channel.[14] In this sense, the incorporation of non-conventional polydentate ligands opens a wide range of structural possibilities.[15] Taking advantage of our studies on solid-state reactivity of olefins as an efficient route for regiocontrolled access to versatile multitopic ligands via [2+2] photocycloadition of olefins, herein, we reported the use of *rctt*-tetracarboxylic acid ($C_8H_8O_8$ = ***rctt*-H$_4$Cbtb**) as the principal building unit for the construction of novel coordination polymers. Our interest in using this acid is due to the possibility of obtaining *in-situ* different geometrical isomers during the synthesis of the materials (see Scheme 1).

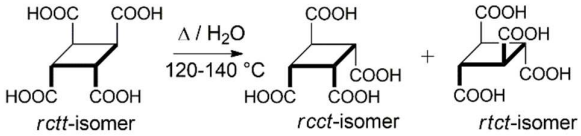

Scheme 1. Reaction diagram to obtain *in-situ* of geometric isomers of ***rctt*-H$_4$Cbtc** acid.

[a] *Laboratorio de Síntesis y Caracterización de Nuevos Materiales, Centro de Química, Instituto Venezolano de Investigaciones Científicas, San Antonio de Los Altos, Miranda, Venezuela. Fax: 58 0212 5041350; Tel: 58 0212 5041609; E-mail: eavila@ivic.gob.ve*
[b] *Laboratorio de Cristalografía, Departamento de Química, Facultad de Ciencias, Mérida, Mérida, Venezuela. Fax: 58 0274 2401290; Tel: 58 0274 2660494; E-mail: marilynelisa6@hotmail.com*
[c] *Laboratorio de Química Computacional, Centro de Química, Instituto Venezolano de Investigaciones Científicas, San Antonio de Los Altos, Miranda, Venezuela. Fax: 58 0212 5041350; Tel: 58 0212 5041741; E-mail: ranez@ivic.gob.ve*
† Electronic Supplementary Information (ESI) available: [Table for X-ray diffraction experimental details and other complementary figure necessary to compressive the discussion of the crystalline structure packing]. See DOI: 10.1039/x0xx00000x

Likewise, the H_4Cbtc molecule provides a wide-variety of metal coordination modes (see Scheme 2) and its coordination chemistry has not been extensively explored.[16] In this contribution, we report the synthesis and structural characterization of three novel coordination polymers based on the combination of ***rctt*-H_4Cbtb** and rigid/flexible ditopic nitrogen heterocycles as secondary units: *trans*-1,2-bis(4-pyridyl)ethane (4,4´-**bpe**). In addition, we will discuss in detail the rationalization of the supramolecular structure formation built-up from Su *et al.,* they suggested two possible steps involved in the coordination polymer's formation mechanism.[17] Besides, to understand what are the different temperature conditions during synthesis with the knowledge of solid-state DFT calculations carried-out on two of the coordination polymers.

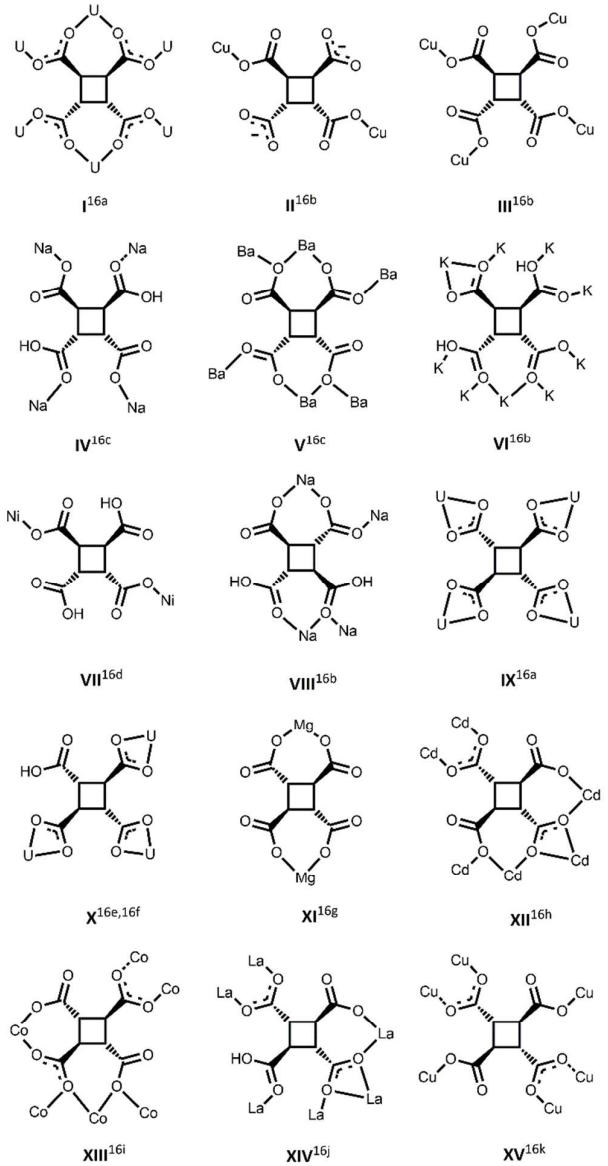

Scheme 2. Different possibilities of coordination for isomers of the ***rctt*-** and ***rtct*-Cbtc**.

Experimental

Chemicals and Methods

The reagents (Aldrich Chemical, Inc., Riedel-de Häen) and solvents, (Merck Co., Baker Analyzed and Eastman Co.) used without further purification.

X-Ray crystallography

Single crystal X-ray diffraction: Compounds 1-3. Suitable single crystals were mounted on a glass fiber and the crystallographic data for **1-3** were selected from reaction conditions at 90 and 120 °C, respectively. All sets of data for each compound were collected at 298(2) K on a Rigaku diffractometer, AFC-7, Mercury CCD-detector, Mo-Kα (λ = 0.71073 Å) radiation. Data collection was performed using ϕ and ω scan. Non-hydrogen atoms are located from the difference E-maps by means of direct methods (*Superflip* software),[18] and the structural data were refined by full-matrix least-squares methods on F^2 using the *SHELXL-2013*,[19] and *SHELXLE*,[20] crystallographic software package. Anisotropic thermal parameters were used to refine all non-hydrogen atoms. The H atoms on the C atoms were included in calculated positions. The H-atoms on water molecules were found from the weak residual electron density peaks. For **2** and **3**, the guest molecules is highly disordered and could not be modeled correctly, so the *SQUEEZE* routine was applied.[21] For this we used the *PLATON* package of crystallographic software.[22] Furthermore, disordered solvent molecules were included in the molecular formula by thermogravimetric and elemental analysis.

X-Ray Powder Diffraction Data: Compounds 1-2. The XRPD patterns were collected on a Bruker Advance D8 or PANalytical X'Pert PRO diffractometer with Cu-*K*α (λ = 1.5418 Å) radiation, with a range in 2θ = 5-70°, step: 0.02° and time: 10s/step. Phase identification and analysis semi-quantitative done with the program *MATCH!* 2, *Crystal Impact*,[23] coupled to patterns' personal database.

Solid-state *ab-initio* calculations. Solid-state optimizations were performed using the Vienna Ab-initio Simulation Program, *VASP*.[24] Kohn-Sham equations were solved with the generalized gradient approximation (GGA) proposed by Perdew and Wang.[25] The projector-augmented-wave (PAW) method of Blöchl[26] in the formulation of Kresse and Joubert[27] were applied to describe electron-ion interactions. The pseudopotentials for Zn, Ni, O, N, C and H have $3d^{10}4s^2$, $3d^9 4s^1$, $2s^2 2p4$, $2s^2 2p^3$, $2s^2 2p^2$ and $1s^1$ valences, respectively. Brillouin-zone sampling was performed on Monkhorst-Pack special points[28] using a Methfessel-Paxton integration scheme. The plane-wave cutoff was set to 450 eV throughout all calculations. Monkhorst-Pack meshes of 6x2x2 and 2x3x4 were enough to give a converged total energy for the **1** and **2**, respectively. Optimization of the atomic coordinates and cell parameters of **1** and **2** were performed using the experimental cell parameters and atomic positions obtained from the X-ray single-crystal diffraction refinement. In compound **3**, the bulk parameters were frozen and only four water molecules were optimized. The cutoff was set to 273.895 eV and a Monkhorst-Pack mesh of 4x6x4 was enough to reach the energy convergence. This methodology has been proven to be useful for studying the structural stability of different coordination polymers.[29]

Elemental Analyses. The C, H and N elemental analyses were conducted on a Fisons-EA1108 CHNS-O elemental analyzer.

IR-FT spectral Analyses. The FT-IR spectra were recorded from KBr pellets in the range 4000–400 cm^{-1} on a Thermo-Scientific FT/IR spectrometer.

Thermal Analyses. TG/DSC analyses were performed on a Mettler-Toledo instrument in flowing N_2 with a heating rate of 10 °C min^{-1}.

General procedure

Synthesis of ligand *rctt*-cyclobutane tetracarboxylic acid (*rctt*-H_4Cbtc). In an agate mortar, imidazole was combined with fumaric acid via mechanochemistry in a 1:1 stoichiometric ratio; both materials were grinding at room temperature for 15 min. Subsequently it was irradiated with UV light for 2-3 days, which allowed obtaining ***rctt*-H_4Cbtc**. This procedure is exactly as the one described for Briceño, *et al.*[30a]

Synthesis of $[Zn_2$(4,4'-bpe)(*rctt*-Cbtc)$(OH_2)]_n \cdot 4H_2O$ (1) and $[Zn$(4,4'-bpe)$_{0.5}$(*rctt*-Cbtc)$_{0.5}(OH_2)]_n$ (2). In a reactor Teflon-lined stainless vessel stoichiometric amounts of ***rctt*-H_4Cbtc** (50.0 mg, 0.22 mmol), $Zn(NO_3)_2 \cdot 4H_2O$ (56.31 mg, 0.22 mmol) and *trans*-1,2-di(pyridin-4-yl) bipyethane), 4,4'-**bpe** (39.68 mg, 0.22 mmol) were added, in 10 mL of water. Subsequently, they were synthetized and placed in an oven at 60, 80, 90, 100, 120, 140 and 180 °C for 72 h (see Table 1). The samples were filtered and were washed repeatedly left finally to dry at room temperature. Colorless crystals type needle and block were filtered off for **1** and **2**, respectively. These crystals washed with distilled water and dried at room temperature. Moreover, for all reactions, the synthesis yield were of 86-90% based on Zn. Elemental analyses only done for **1** with molecular formula $C_{20}H_{26}O_{13}N_2Zn_2$, because this was obtained in a 86% a as pure form, as indicated in Table 1 and Fig. 1. **Elemental analysis for 1:** Anal. Calcd. (%): C, 37.94; N, 4.42; H. 4.14. Found (%): C, 37.67; N, 4.34; H, 3.71. FT-IR (KBr pellet, cm^{-1}): 3370 (s), 1619 (s), 139184 (s), 1289 (m), 1230 (m), 1030 (m), 833 (m), 672 (m).

Synthesis of $[Ni_2$(4,4'-bpe)$_2$(*rctt*-Cbtc)$(OH_2)_2]_n \cdot 4H_2O$ (3). To obtain this compound, a mixture of ***rctt*-H_4Cbtc** (0.05 g, 0.21 mmol), 4,4'-**bpe** (0.039 g, 0.21 mmol), $Ni(NO_3)_2 \cdot 6H_2O$ (0.063 g, 0.22 mmol) and 10 mL of deionized water were sealed in a Teflon-lined stainless vessel and heated at 100 °C for 72 h, then cooled slowly to room temperature. Light blue crystals of **3** were formed, which were washed with water and dried in air. Yield: 85%. **Elemental analysis:** Anal. Calcd. (%): C, 41.32; N, 6.02; H 5.63. Found (%):C, 42.62; N, 6.06; H, 5.16. FT-IR (KBr pellet, cm^{-1}): 3362 (s), 1564 (s), 1391 (s), 1289 (m), 1226 (m), 1026 (m), 823 (m), 642 (m).

Table 1. Semi-quantitative analysis, in percentage (%), of **1** and **2** as the final product at different temperature of synthesis.

Exp.	Temp./°C	1%	2%	Imp.%
1	60*	75.0	-	25.0
2	80$	100.0	0.0	-
3	90$	100.0	0.0	-
4	100$	92.5	7.5	-
5	120$,*	57.7	42.3	20.0
6	140$,*	82.7	17.3	85.0
7	180	0.0	0.0	100.0

($) Percentage values for **1** and **2** were obtained using the program Match 2! Nevertheless, (*) values correspond with those calculated from the impurities, based on the ratio between the intensity of the most intense Bragg reflection, the 100, for compound **1** and the most intense one for the impurity.

Molecular and Crystalline Structure.

In order to explain the rather intricate network motifs of the supramolecular structures of **1-3**, we carried out a topological study with the *TOPOS 4.0* software.[31] In compounds **1** and **2** the oxidation states of Zn ions were confirmed by charge neutrality, coordination environments, and valence sum calculations.[32] The detailed conformations of 4,4'-**bpe** ligands in these compounds are shown in Table S2. ESI†.

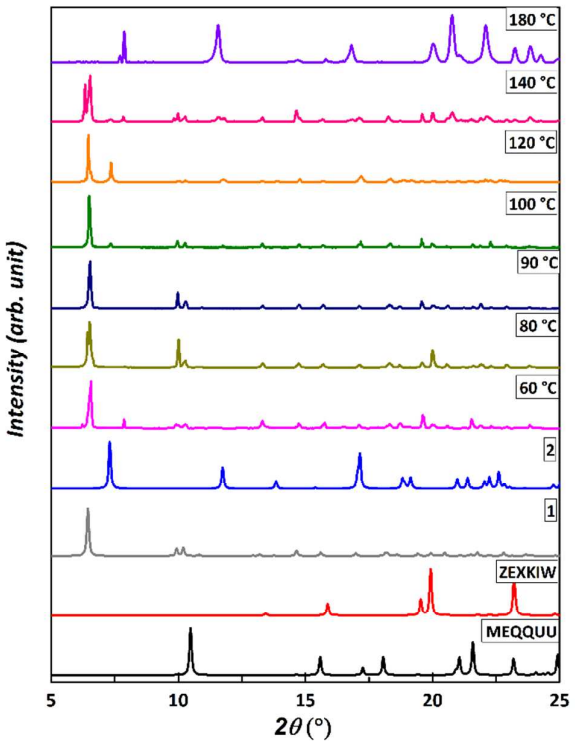

Fig. 1. Powder patterns for mixtures of **1** and **2** in the final product at different temperatures of synthesis. For identification purposes, also shown are the simulated powder patterns of the starting materials: *rctt*-H_4Cbtb (CSD code: MEQQUU)[34] and 4,4'-**bpe** (CSD code: ZEXKIW)[35], and simulated powder patterns 1_S and 2 for **1** and **2** obtained from the single crystal structures and crystallographic data derived from this work. The 180 °C 3 days experiment shows an unknown phase that could not be indexed.

Discussion

Compounds 1 and 2

Single-crystal X-ray diffraction analysis of compounds **1** and **2** reveals that they crystallize in monoclinic space groups $P2_1/c$ and $P2/c$, with asymmetric units containing $[Zn_2$(4,4'-**bpe**)(***rctt*-Cbtc**)$(OH_2)]_n \cdot 4H_2O$ (see Fig. 2a, 2b) and $[Zn$(4,4'-**bpe**$)_{0.5}$(***rctt*-Cbtc**$)_{0.5}(OH_2)]_n$ (see Fig. 3), respectively.‡ Compound **1** has two crystallographically independent Zn ions. Zn1 is surrounded by two ***rctt*-Cbtc** ligands, with one of them acting as a chelate (through $O3^i$ -equatorial- and O6 -axial-, with distances Zn1—$O3^i$ 1.997(2) Å and Zn1—O6 2.090(2) Å, respectively), while the other acts as a monodentate ligand (through O1-axial-, with distance Zn1—O1 1.963(2) Å). In addition, Zn1 coordinates to a 4,4'-**bpe** ligand (N1 bonded in equatorial position, with distance Zn1—N1 2.025(2) Å) and to a water molecule (through OW -axial-, with distance Zn1—O2W 2.358(2) Å). This environment represents a coordination sphere of a distorted trigonal bipyramid for Zn1. Zn2 is surrounded by three ***rctt*-**

Cbtc ligands, each one acting as a monodentate ligand by means of the carboxylate groups directly participating through O4, O5 and O7 (with distances Zn2—O4 1989(2) Å, Zn2—O5 1.977(2) Å and Zn2—O7 1.951(2) Å, respectively). In addition, a 4,4'-**bpe** ligand bounds Zn2 via N2, with distance Zn2—N2^{ii} 2.035(2) Å. This environment around Zn2 describes a tetrahedral coordination sphere, as illustrated in Fig. S2, ESI†. It is interesting to note that two of the four carboxylic acids of the ***rctt*-Cbtc** ligand display C—O bond distances similar within 3 u.s. (see Table S1, ESI†), these values suggest that such carboxylates groups share the negative charge between the two C—O bonds via resonance. Exactly, those two involved in the chelate binding bite to Zn1 ions through O3 and O6. Furthermore, they bond to Zn2 ions through the other O atoms of the carboxylates, O4 and O7, acting as bridges between Zn1 and Zn2 ions (see Fig. S2c, ESI†).

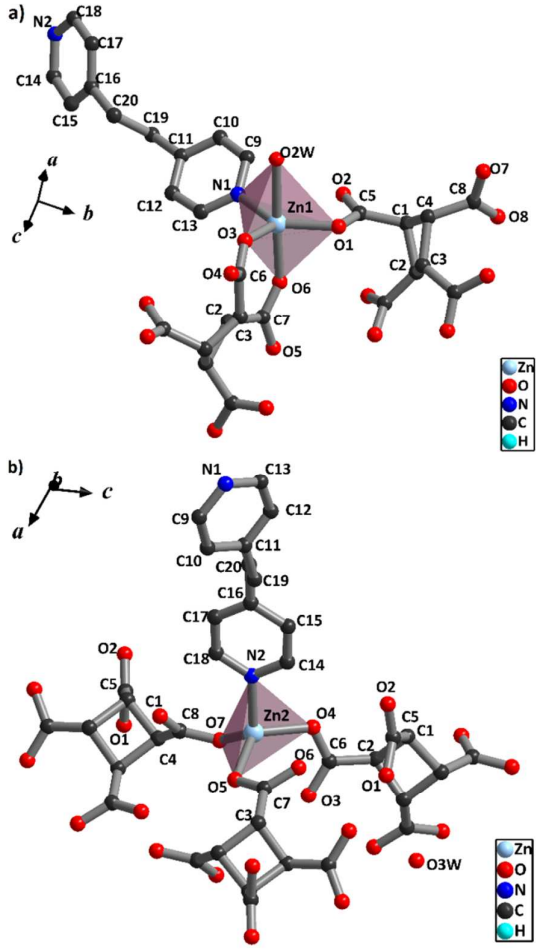

Fig. 2. Asymmetric unit of **1** (a,b) showing atom-labeling. (a) and (b) show views of bipyramid trigonal and tetrahedral coordination spheres of Zn1 and Zn2 ions, in compound **1**.

Compound **2** has only one crystallographically independent ion Zn1 in contrast to **1**, whose environment consists of two ***rctt*-Cbtc** ligands, one 4,4'-**bpe** ligand and one water molecule. The first bind to the ion Zn1 through as monodentate carboxylate groups through O1 and O4 atoms with bond distances Zn1—O1 1.997(2) Å and Zn1—O4 1.929(2) Å, respectively. In turn, the Zn1 ion is bound to the N1 atom with bond distance Zn1—N1 2.011(3) Å; finally, O1W bonds the metal, with distance Zn1—O1W 2.045(2) Å. This describes a tetrahedral coordination sphere around the Zn1 ion, as illustrated in Fig. S3a, ESI†. In **1** and **2**, the cyclobutane ring in the ***rctt*-Cbtc** ligands show an envelope conformation described by the Cremer-Pople puckering parameters.[33] Additionally, the ***rctt*-Cbtc** ligands in both structures display two new type linking modes, according to Scheme 3.

Furthermore, in both structures the 4,4'-**bpe** ligands display different structures as described by the torsion angle about the bond C19—C20 [C11—C19—C20—C16] in **1**, being equal to 168.3(4)° and thus adopting an *anti*-conformation; while the equivalent torsion angle in **2**, C3—C6—C6^{i}—C3^{i} equals -49.9(6)° (Fig. S1a, ESI†), adopting a *gauche* conformation. A Mogul 1.4[36] search in the CSD[37] showed 960 observations for 601 coordination polymer structures which display at least one 4,4'-**bpe** ligand, with R-factors less than 7.5. We found that the predominant conformation for the 4,4'-**bpe** is the *anti* conformation (see Fig. S1b, ESI†), which represents 460 observations whose values are around 180°.

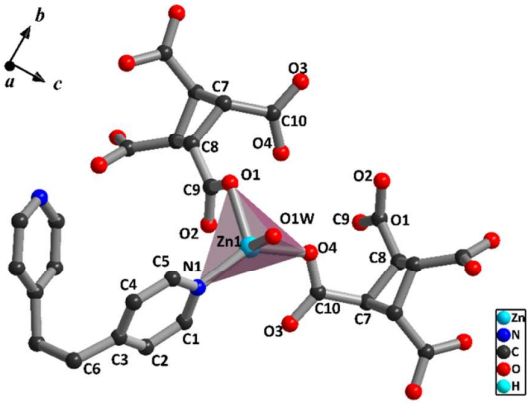

Fig. 3. Asymmetric unit of **2** showing atom-labeling and tetrahedral coordination sphere for Zn1 in compound **2**.

The supramolecular structure of **1** shows Zinc polioxocarboxylate layers extending along (100)-plane. Likewise, layers are separated from each other by one translational unit along the *a*-axis, where each 4,4'-**bpe** ligand acts as bridging links between Zn1 and Zn2 of adjacent parallel layers. These extended layers have two types of supramolecular rings. First, one with 11 members: Zn1—O1—C1—C2—C5—C6—O4—O5—Zn2—O6—C7, and the other with 14 member: Zn2—O5—C7—C3—C4—Zn2—O7—C8—O5—C3—C4—C7—C8—O7 (see Fig. S4, ESI†). Consequently, in the [010]-direction there are pores with dimensions Zn···Zn of 13.145(3) x 4.641(5) Å, as illustrate in Fig. S5a. These cyclic structures extending along the *b*-axis generate 1-D zigzag channels of dimensions Zn···Zn of 13.145(3) Å x 9.2627(1) Å (see Fig. S5b, ESI†). Moreover, compound **2** is comprised by a parallel arrangement of supramolecular chains made of 14-membered rings: Zn1—O1—C9—C8—C7—C10—C4—Zn1—O1—C9—C8—C7—C10—C4, which run along [001]-direction, as shown in Fig. S6, ESI†.

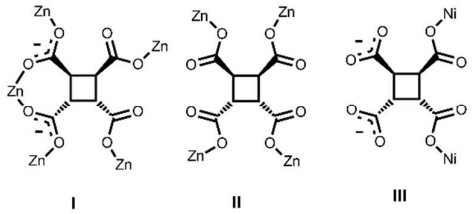

Scheme 3. Three new type-linking modes for ***rctt*-Cbtc**.

In turn, these structures are connected through the 4,4'-**bpe** ligand producing a helical chains that runs in the [100]-direction, interconnecting Zn1···Zn1 ions via links with carboxylate groups and the cyclobutane ring (see Fig. 7S, ESI†). In this way, such an arrangement leads to the formation of supramolecular layers extending along (010)-plane stacked and joined by van der Waals interactions, as illustrated in Fig. 5b. Interesting to note the similarities between the structures of **1** and **2**. The 14-member rings are observed in both compounds, and their superposition show *rms* deviations less than 0.714 Å. Therefore, these pre-organized supramolecular structures are kept intact while compound **1** evolves into compound **2**. Another striking similarity is their H-bond patterns. Compound **1** display extended chains that run along *bc*-plane composed of two types of H-bonds. One forming rings described by graph set $R_4^4(12)_{O7}$ replicated along [011]-direction (see Fig. 6). The other corresponds to extended lineal chains running along [010]-direction, described by graph set $C_4^4(10)_{O2W}$. Combination of both graph sets gives $C_3^3(10)_{O2W}[R_4^4(12)_{O7}]$, which predominantly describes-bonds patterns along [010]-direction.

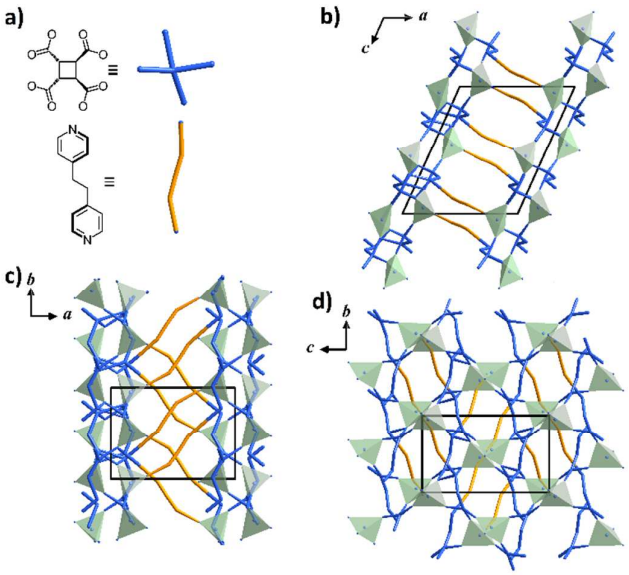

Fig. 4. (a) Schematic representation of the ligands 4,4´-**bpe** and ***rctt*-Ctbc** seen as the simplified structure for compound **1** generated by the program TOPOS 4.0. (b) View of the projection on the *ac*-plane showing the openings of 1-D channels of dimensions: 13.145(3) x 4.641(5) Å and generated by the coordination of Zn1 and Zn2 ions with the organic ligands. (c) and (d) represent the crystal packing for the projections on the *ba* and *cb*-planes, respectively. Additionally, (b) and (c) show polioxocarboxylate layers in the *cb*-plane separated by a unitary translation along *a*-axis.

Compound **2**, shows also graph set $R_4^4(12)_{O7}$ running this time along [011]-direction (see Fig. 7). The second graph $C_4^4(10)_{O2W}$, corresponds to a chain running along [010]-direction. Both descriptors produce a unified symbol $C_3^3(6)_{O2W}[R_4^4(12)_{O7}]$, which describes an extended arrangement of H-bonds along [010]-direction. Finally, empty space calculations using Mercury CSD 3.3 (build RC5)[38] were performed using the contact surface and accessible solvent approximations using test ratio and lattice space equal to 1.2 and 0.7 Å, respectively. This evaluation gave 429.37 $Å^3$ (representing 16.9% of unit cell volume) and 77.96 $Å^3$ (representing 3.1% of unit cell volume), respectively.

Temperature effects: Phases formation under hydrothermal conditions.

The XRPD patterns in Fig. 1 show that compound **1** is observed as a single phase up to 90 °C, when the reaction was carried out at high temperatures: 100, 120, 140, and 180 °C. Then, the concomitant formation of **1** and **2** occurs in the temperatures range between 100-140°C at different ratios, as indicated in Table 1, observing a relative decrease of **1** to 100 °C with percentage of 25, in comparison with the formation of **2** at the same temperature. The phases **1** and **2** disappear completely when the reaction is carried-out at 180°C, as outlined in Table 1. It is also observed that a novel unidentified phase appears. This new phase could contain a novel isomer ***rtct*-H_4Cbtc**, which is favored at temperatures above 140 °C (see Fig. 8S).[16c,30] It is worth that **2** contains similar Zn(II)/Cbtc/4,4'-**bpe** molar ratio (2:1:1) with respect to **1**. This chemical feature suggests that both compounds could be considered as a singular case of supramolecular isomers[39] that let us to infer that the formation of **1** and **2** are conditioned by thermodynamic or kinetic control. These results prompted us to evaluate the influence of the reaction time and temperature to verify if the structure **2** is derived from **1**.

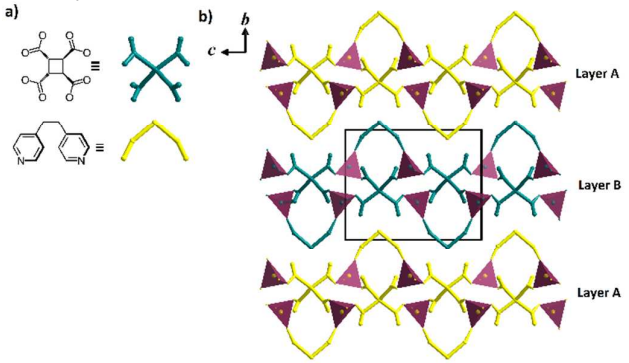

Fig. 5. (a) Schematic representation of the ligands 4,4´-**bpe** and ***rctt*-Ctbc** in the crystal structure of compound **2** with TOPOS 4.0. (b) This is view on the *bc*-plane showing extended 2-D supramolecular layers, which are interdigitated following the sequence ABA and joined by van der Waals interactions.

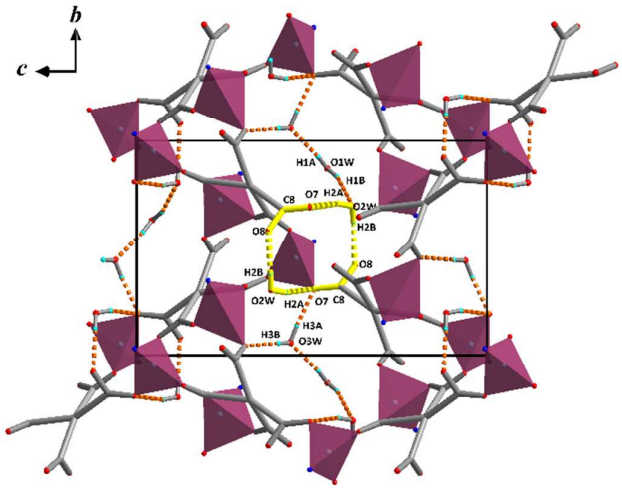

Fig. 6. H-bonding packing for **1** showing the 12-members ring (highlighted in yellow) corresponding to graph set $R_4^4(12)_{O7}$.

At this point, it is important to highlight that the hydrothermal synthesis of the coordination polymers, in general, kinetic products are favored as metastable phases, due to the conditions of temperature and pressure generated autogenously inside the hydrothermal bomb.[40] Therefore, the self-assembly of precursors to yield the coordination polymers results from the solubility they display under hydrothermal conditions. As in zeolites, the kinetic states play an important role in the determination of the final products.[41] That is why to control the kinetic states during the self-assembly of the coordination networks around the metal centers is fundamental to understand the steps taken towards their formation and stabilization. Nevertheless, in contrast with zeolites where this important feature is widely discuss, with coordination polymers there is a lack of information in the literature concerning this issue.[6a,13,41]

Thus, we performed three experiments to verify if compound **1** transforms into **2**. This was done starting with the reaction product obtained under the experimental conditions (80° C, 3 days) in which we obtained pure **1**. This was divided into three parts; a third of it was taken and added to a reactor Teflon-lined stainless vessel with 10 mL of distilled water and subjected to 80° C for 5 days in an oven. Second, we took another third of the material, which was added into a reactor Teflon-lined stainless vessel, with 10 mL of distilled water and subjected to a reaction time of 3 days at 100° C. Finally, the remaining third part of the material was taken and we proceeded in the same manner as the previous reactions, but with reaction, temperature and time equal to 100° C and 5 days, (see Table 2, Fig. 8).

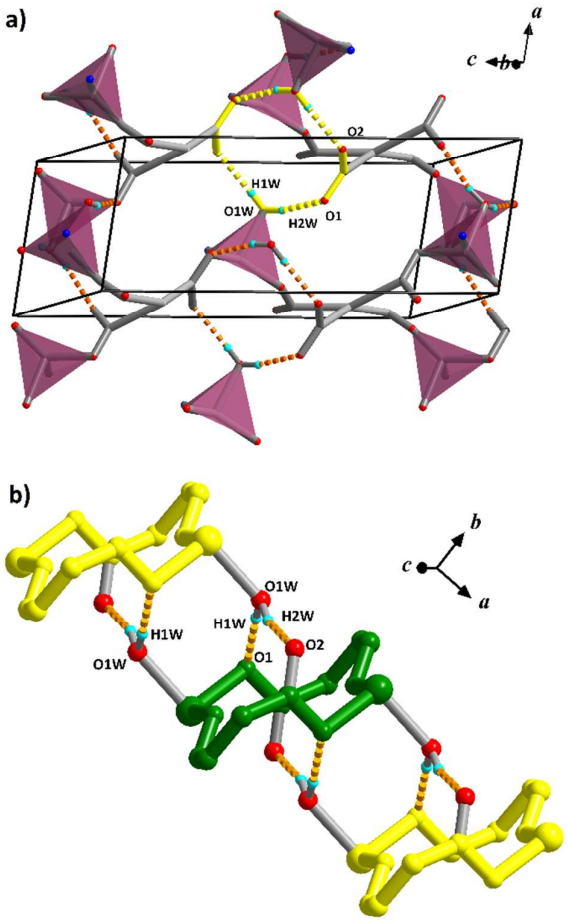

Fig. 7. (a) H-bonding packing for **2** showing the 12 members ring (highlighted in yellow) corresponding to graph set $R_4^4(12)_{O7}$. (b) H-bonding packing for **2** showing the 12 members ring corresponding to graph set $C_3^3(10)_{O2W}[R_4^4(12)_{O7}]$.

After heating, the reactors were allowed to cool slowly to room temperature and XRPD patterns were recorded from the resulting solids. The XRPD confirmed in three of four cases the presence of concomitant phases **1** and **2**. It is interesting to note that such transformations appear to be reached more rapidly when the time reaction is increased to 5d at either 80 °C or 100 °C, observing a significant conversion of **1** into **2** in a percentage of 73.9:26.1 to 15.7:84.3, respectively. Whereas, an increase of temperature keeping the reaction time in 3d caused the conversion in a minor proportion 93.6:6.4 at 100 °C. Such results suggest that the formation of **1** is the thermodynamic product most stable with respect to **2**.

Su *et al.,* suggested two possible steps involved in the coordination polymer's formation mechanism.[17] The first step is an implies the polymerization of species with supramolecular structures of open rings; for example, the *anti* conformation of the ligand 4,4'-**bpe** to give rise to pore structures of dimensions Zn···Zn of 13.145(3) x 4.641(5) Å. The second one implies the cyclization of oligomeric intermediaries that produce "discrete rings": for example, the *gauche* conformation of the ligand 4,4'-**bpe** which allows interconnecting Zn1···Zn1 ions and giving rise to extended pile up layers linked by van der Waals interactions (as showed in Fig. 5b).

Table 2. Reaction conditions and percentage value for semi-quantitative analysis of **1** and **2** in the final product mixture.

Exp.	Temp./°C	Time/d	1%	2%
Initial	80	3	100.0	0.0
1	80	5	73.9	26.1
2	100	3	93.6	6.4
3	100	5	15.7	84.3

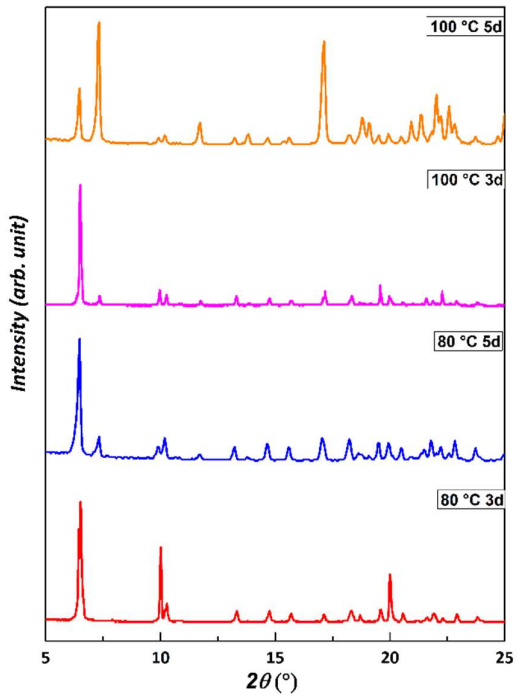

Fig. 8. X-ray powder diffraction patterns for the final mixed compounds **1-2**; in accord with the initial, 1, 2, and 3 experiments obtained under reaction conditions shows in the Table 2.

Thermal stability analysis for compound 1

To examine the thermal stability as a function of temperature of compound **1**, because of its condition of pure phase (see Table 1), we performed a thermal gravimetric analysis (TGA). The TGA curve (see Fig. S10, ESI†) shows that the first weight loss of 12.80% happening in the range 39.66-106.97 °C, corresponds to the loss of four water molecules (calculated $4{\cdot}H_2O$ = 11.37 value %). This transition is associated with the dehydration of the material. A second weight loss of 43.07% observed from 180.10-508.18 °C indicates decomposition of the organic ligands. Finally, it is seen that **1** is thermally stable up to 380 °C.

Solid-state calculations for compounds 1 and 2

Table 3 displays the optimized bulk parameters for **1** and **2**. The geometric parameters obtained for both **1** and **2** bulks are in good agreement with the experimental values showing a deviation with respect to the experimental data less than 2%. In order to compare the bulk stabilities and due to the fact that the two structures possess the same type of atoms, we calculated the bulk total energy normalized to the total atom number (**1** and **2** have 204 and 108 atoms, respectively). The normalized energies for **1** and **2** are -6.20 and -6.35 eV, respectively, which indicates that from a thermodynamic point of view, the 2-D packing is a little more stable than the 3-D packing at low temperature. As was mentioned before, water is binding to the Zn atoms in both structures and in greater amount in the structure **2**. By supposing that equilibrium between the two structures exists, some water molecules must leave the coordination sphere of the structure **2** to form the structure **1**. Then we evaluated the interaction energy of one water molecule with a Zn atom in the structure **2** Two calculations were carried out, an adiabatic calculation where the structure was frozen without the water molecule and one calculations where all atoms were optimized. The adiabatic calculation gives an idea of the interaction energy between the water molecule and the Zn atom without taking into account the relaxation of the structure. The difference between the adiabatic calculation and the full optimization calculation offers important insight about the energy involved in the structure transformation due to the loss of one water molecule. The calculated interaction energy between the water molecule and the Zn atom in the adiabatic system is -1.61 eV, that is, the system losses energy when water leaves the coordination sphere of the Zn atom. After the optimization process, the system gains 0.65 eV that is 40% of the energy lost in the adiabatic calculation.

Table 3. Optimization bulk parameters for **1** and **2**.

Parameters	**1**		**2**	
	Exp.	Theo.	Exp.	Theo.
a/Å	15.023	15.067	5.844	5.924
b/Å	10.164	10.108	12.088	12.274
c/Å	18.196	18.321	15.288	15.458
β/°	114.233	113.410	99.975	99.291

The most significant structural change due to the optimization process is observed in the interaction between the Zn atom (that lost the water molecule) and one of its ***rctt*-Cbtc** ligand. After the bulk calculation, the two ***rctt*-Cbtc** ligands are bonded to the Zn atom by one oxygen atom with interaction distances of 2.03 and 1.94 Å. After the optimization process without the water molecule, the ***rctt*-Cbtc** ligand bonded at 2.03 Å is now interacting with the two oxygen atoms at distances of 2.11 and 2.14 Å. Despite the interaction between the ***rctt*-Cbtc** and the Zn atom decreased, as suggest the increased in the interaction distances, these results clearly indicate that vacancies left by the water molecules could be satisfied by interaction with the oxygen atoms of the ***rctt*-Cbtc** ligands. Then, the change from a 2-D to a 3-D packing could improve the interaction between the O (of the ***rctt-Cbtc*** ligands) and the Zn atoms increasing the energy gains by the system when water molecules left the coordination sphere. In fact, the average distances among the oxygen atoms of the ***rctt*-Cbtc** ligands which form bridges between Zn atoms in the structure **1** is 2.05 Å indicating the greatest interaction and why the higher stability of the structure **1** despite the exothermic behavior when water leaves the coordination sphere of the Zn atoms.

Compound 3

This crystallizes in the monoclinic space group *P*2*/c* and its asymmetric unit contains a half of a $[Ni_2(4,4'\text{-}\mathbf{bpe})_2(\mathbf{rctt\text{-}Cbtc})(OH_2)_6]$ molecule and three H_2O solvent molecules.‡ The Ni(II) atom has a distorted octahedral coordination geometry.

This being coordinated by two N atoms of two 4,4'-**bpe** ligands with bonds distance Ni1—N1 2.073(2) Å and Ni1—N2 2.082(2) Å. Also, an O atom of a unidentate carboxylate group of a ***rctt*-Cbtc** ligand [Ni1—O1 2.066(2) Å] and by three O atoms of H_2O molecules [Ni1—O1W 2.074(2) Å, Ni1—O2W 2.104(2) Å, Ni1—O3W 2.113(2) Å], as illustrated in Fig. 9. The 4,4'-**bpe** ligand is capable of adopting either gauche or anti conformations and can therefore act as either an angular or linear spacer ligand, respectively. In compound **3**, the 4,4'-**bpe** ligand adopts the gauche conformation with torsion angle equal to 69.5(3)°. Moreover, the ligand ***rctt*-Cbtc** adopts an envelope conformation according to the Cremer-Pople puckering parameters,[33] and displays a binding new type mode shown in scheme 3.

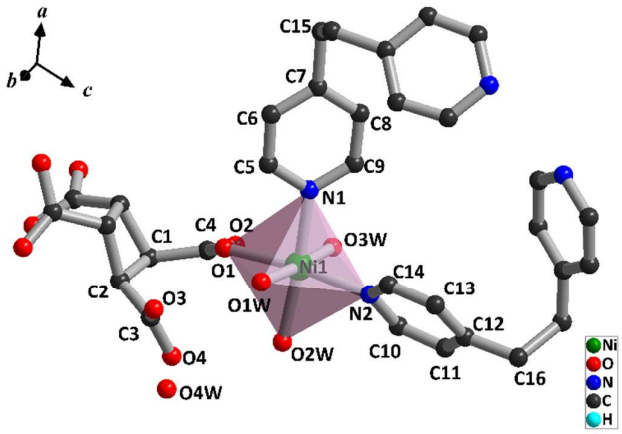

Fig. 9. Asymmetry unit of **3** showing the atom-labeling and view of coordination sphere of Ni1 ion.

Each 4,4'-**bpe** ligand bridges Ni(II) ions to forms a small grid with dimensions of 6.97 x 7.05 Å. These small grids linked through the ***rctt*-Cbtc** ligands forming 1-D chains that runs along [101]-direction as illustrated in Fig. 10. The intrachain distance Ni···Ni is 9.18 Å. Although this chain creates a small grid, the displaced stacks of 1-D chains contain no 1-D channels. Among the neighboring chains, there are located water molecules that through intermolecular interactions of hydrogen bonds generate 2D layers along *b*-axis.

Compound **3** presents a supramolecular arrangement of box type H-bonds as is displayed in the Fig.11, and whose graph set is not described easily because 5 different types of H-bonds forming chains extend along the *b*-axis represent it. This H-bonds can be described with the following sets of graphs: $2R_4^2(8)_{O1W}$, $2R_4^2(8)_{O3W}$, $R_2^2(8)_{O1W}$, $R_2^2(8)_{O1W}$, and $C_2^2(11)_{O3W}$, originating different supramolecular arrangements in the form of rings. Finally, a set of graphs of the type $C_2^2(7)_{O3W}[2R_4^2(8)_{O3W}]$, predominantly describes a arrangement extended as shown in Fig. 11.

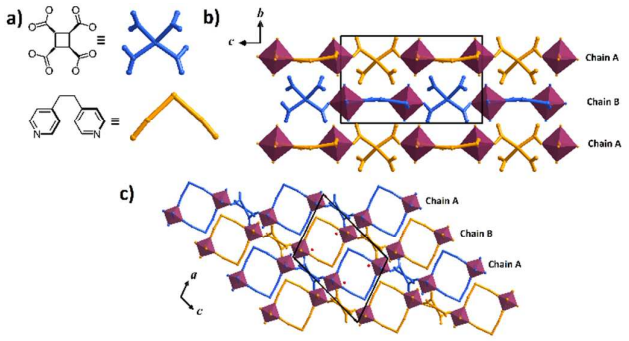

Fig. 10. (a) Schematic representation of the ligands 4,4´-**bpe** and ***rctt*-Ctbc** in the simplified structure derived from the program TOPOS 4.0 for compound **3**. (b) and c) Views down the *bc* and *ac*-planes, respectively. These projections show how the 1-D chains piled up in a sequence type ABA are joined by H-bonds.

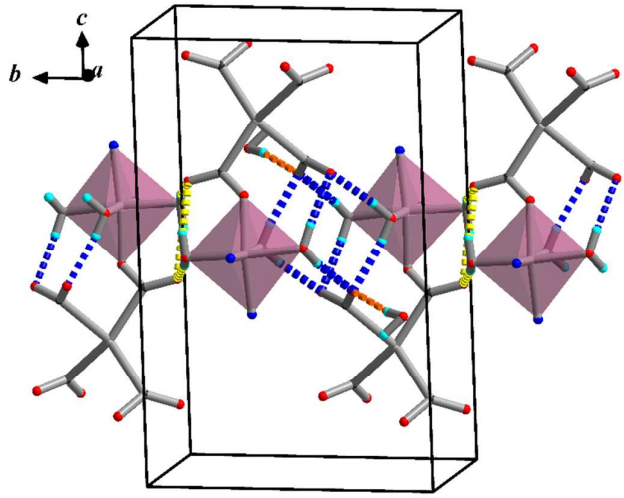

Fig. 11. H-bonding packing for **3** showing of box type supramolecular structure constituted by 12 members ring corresponding to graph set $C_3^3(6)_{O2W}[R_4^4(12)_{O7}]$.

Thermal stability analysis for compound 3

For **3**, the TGA curve shows, as illustrated in Fig. 12S, ESI†, that the first weight loss of 17.67%, occurring from 39 °C to 205 °C, corresponds to the loss of solvent molecules (calculated 23.24%). A second weight loss of 58.25% observed from 206 to 467 °C that indicates decomposition of the organic ligands (calculated 56.14%).

Solid-state calculations for compound 3

Following the methodology described by Kaduk[42] to describe in the best way the H-bond packing of compound **3**, we performed calculations to determine the orientation and position of the water molecule labeled as O4W due to the fact that the hydrogen atoms of this water molecule were not located in the final difference Fourier map of the refined structure.[43] The final results show that the water molecule O4W acts as a bridge between water molecule O3W and the metal center Ni1, the other hydrogen atom of O4W bonds to the O4 of one of the free carboxylates, making it a trifurcated hydrogen acceptor (see Fig. S13, ESI†).

Conclusions

In this work, we report three new coordination polymers that were successfully isolated and characterized by X-ray diffraction, and were obtained due to the versatility displayed by both ligands: the free rotation of the carboxylate groups (***rctt*-Cbtc**) and of the pyridine groups (4,4'-**bpe**). Furthermore, we were able to obtain coordination polymers with 3-D, 2-D and 1-D topologies for compounds **1**, **2** and **3**, respectively. Additionally, the versatility of the ligand ***rctt*-Cbtc** to coordinate metal centers and satisfied efficiently the metal charge were studied, such as for Zn ions in compounds **1** and **2**, and for Ni ions in **3**, as shown in Scheme 3. In addition, these new three types of binding modes added up to the fifteen existing modes, according to Scheme 2. On the other hand, the ligand 4,4'-**bpe** display restricted geometries depending on temperature; it display an *anti* conformation in the case of compound **1**, and a *gauche* conformation for compounds **2** and **3**, which were obtained at higher temperature (100 °C) than for **1** (80 °C). Moreover, compounds **1**-**2** provide an example of concomitant phases existing under hydrothermal conditions. We were able to rationalize the possible environments that enable the formation of compound **2** starting from compound **1** by incrementing temperature or reaction time. In that sense, we found both compounds **1** and **2** displayed a 14-member supramolecular ring with a *rms* of 0.714 Å when they were superimposed, which let us know that they remain intact regardless of the hydrothermal conditions to produce either **1** or **2**. Hence, the H-bond pattern for both compounds is very similar. It is likely that this supramolecular structure is stable enough to preserve itself during the transition from **1** to **2**. So that, the interconversion of **1** to **2** is given for two possible steps involved in the coordination polymer's formation mechanism.[17] Compounds **1–2** provide an uncommonly example of solids that are involved in transformations with preservation of the same building block composition in which a pre-assembled phase is transformed to a related phase, making possible to prepare unprecedented examples of metastable phases. Only compounds **1–2** were observed at temperatures below 140 °C, being compound **2** the thermodynamically more stable. However, at 180 °C, such phases correspond to transient phases prior to the formation of a novel phase thermodynamically more stable, which was unidentified in this work. Nevertheless, we believe that it has as ligand the isomer ***rtct*-Cbtc**. Finally, DFT calculations corroborate the experimental observations; compound **2** is a few more stable than **1** at low temperature. The energy lost when water leave the Zn atom is partially compensated by the O atom of the ***rctt*-Cbtc** ligand and could induce the formation of compound **1** when water leaves the coordination sphere of the Zn atom.

Acknowledgements

This study was financial supported by the FONACIT (grant LAB-97000821 and PEII-2011001110). We are grateful to Lic. Miguel Angel Ramos for data collecting powder diffraction facilities of *Laboratorio de Difracción de Rayos-X y Fluorescencia*-INZIT (G-20050000433), Zulia-Venezuela. In addition, we wish to thank Lic. Blas Delgado, Support Researcher I&D, for data collecting powder diffraction facilities of *Gerencia General Soporte Tecnológico*, PDVSA-INTEVEP, Miranda-Venezuela. Finally, we also want to thank to Lic. Dayana Leal, she is part of our research group, for the interpretation of ^{1}H-NMR spectra.

Notes and references

‡ CCDC 1004887, CCDC 1004888, CCDC 1028267 for compounds **1**, **2**, and **3**, respectively, contains the supplementary crystallographic data for this paper. These data can be obtained free of charge from The Cambridge Crystallographic Data Centre via www.ccdc.cam.ac.uk/data_request/cif.

1 (a) Y. Kobayashi, B. Jacobs, M. D. Allendorf and J. R. Long, *Chem. Mater.*, 2010, **22**, 4120–4122; (b) M.-H. Zeng, Q.-X. Wang, Y.-X. Tan, S. Hu, H.-X. Zhao, L.-S. Long and M. Kurmoo, *J. Am. Chem. Soc.*, 2010, **132**, 2561–2563; (c) R. E. Morris and X. Bull, Nat. Chem., 2010, 2, 353–361; (d) H. Li, M. Eddaoudi, M. O'Keeffe and O. M. Yaghi, *Nature*, 1999, **402**, 276-279; (e) S. S.-Y. Chui, S. M.-F. Lo, J. P. H. Charmant, A. G. Orpen and I. D. Williams, *Science*, 1999, **283**, 1148-1150.

2 (a) G. Férey, *Chem. Soc. Rev.*, 2008, **37**, 191–214; (b) M. D. Allendorf, C. A. Bauer, R. K. Bhakta and R. J. T. Houk, *Chem. Soc. Rev.*, 2009, **38**, 1330–1352; (c) M. Du and X.-H. Bu, *Bull. Chem. Soc. Jpn.*, 2009, **82**, 539–554.

3 (a) A. Corma, H. Carcía and F. X. L. I Xamena, *Chem. Rev.*, 2010, **110**, 4606–4655; (b) L. Ma, C. Abney and W. Lin, *Chem. Soc. Rev.*, 2009, **38**, 1248–1256; (c) J. Y. Lee, O. K. Farha, J. Roberts, K. A. Scheidt, S. B. T. Nguyen and J. T. Hupp, *Chem. Soc. Rev.*, 2009, **38**, 1450–1459; (d) A. U. Czaja, N. Trukhan and U. Müller, *Chem. Soc. Rev.*, 2009, **38**, 1284–1293.

4 (a) M. Kurmoo, *Chem. Soc. Rev.*, 2009, **38**, 1353–1379; (b) D. Maspoch, D. Ruiz-Molina and J. Veciana, *Chem. Soc. Rev.*, 2007, **36**, 770–818; (c) O. Sato, J. Tao and Y.-Z. Zhang, *Angew. Chem., Int. Ed.*, 2007, **46**, 2152–2187.

5 (a) H. Sakamoto, R. Matsuda, S. Bureekaew, D. Tanaka and S. Kitagawa, *Chem.–Eur. J.*, 2009, **15**, 4985–4989; (b) D.-F. Sun, S.-Q. Ma, J. M. Simmons, J.-R. Li, D.-Q. Yuan and H.-C. Zhou, *Chem. Commun.*, 2010, **46**, 1329–1331; (c) C.-P. Li, X.-H. Zhao, X.-D. Chen, Q. Yu and M. Du, *Cryst. Growth Des.*, 2010, **10**, 5034–5042.

6 (a) M. C. Bernini, F. Gándara, M. Iglesias, N. Snejko, E. Gutiérrez-Puebla, E. V. Brusau, G. E. Narda and M. Á. Monge, *Chem.–Eur. J.*, 2009, **15**, 4896–4905; (b) L.-S. Long, *Cryst. Eng. Comm*, 2010, **12**, 1354–1365; (c) C.-P. Li, Q. Yu, J. Chen and M. Du, *Cryst. Growth Des.,* 2010, **10**, 2650–2660; (d) B. Zheng, H. Dong, J.-F. Bai, Y.-Z. Li, S.-H. Li and M. Scheer, *J. Am. Chem. Soc.*, 2008, **130**, 7778–7779.

7 (a) M. Du, C.-P. Li and J.-H. Guo, *Cryst. Eng. Comm.*, 2009, **11**, 1536–1540; (b) C. S. Campos-Fernández, B. L. Schottel, H. T. Chifotides, J. K. Bera, J. Bacsa, J. M. Koomen, D. H. Russell and K. R. Dunbar, *J. Am. Chem. Soc.*, 2005, **127**, 12909–12923; (c) C.-P. Li and M. Du, *Inorg. Chem. Commun.*, 2011, **14**, 502–513.

8 M. Munakata and S. Kitagawa, *Inorg. Chim. Acta*, 1990, **169**, 225–234.

9 M. J. Weaver and G. E. McNis, *Acc. Chem. Res.*, 1990, **23**, 294–300.

10 (a) P. F. Barbara and W. Jarzeba, *Acc. Chem. Res.*, 1988, **21**, 195–199; (b) G. Cainelli, P. Galletti and D. Giacomini, *Chem. Soc. Rev.*, 2009, **38**, 990–1001; (c) B. Bagchi and B. Jana, *Chem. Soc. Rev.*, 2010, **39**, 1936–1954.

11 (a) M. P. Patil and R. B. Sunoj, *Chem.–Eur. J.*, 2008, **14**, 10472–10485; (b) G. B. Dutt, Chem. Phys. Chem., 2005, **6**, 413–418; (c) C. A. Hunter, *Angew. Chem., Int. Ed.*, 2004, **43**, 5310–5324.

12 S. Funahashi and Y. Inada, *Bull. Chem. Soc. Jpn.*, 2002, **75**, 1901–1925.

13 G. K. Kole and J. J. Vittal, *Chem. Soc. Rev.*, 2013, **42**, 1755-1775.
14 S. Noro, S. Kitagawa, M. Kondo and K. Seki, *Angew. Chem., Int. Ed.*, 2000, **12**, 2081-2084.
15 (a) A. Briceño, A. Fulgence, Y. Hill and R. Atencio, *Dalton Trans.*, 2008, 3275-3278; (b) Y. Hill, M. Linares and A. Briceño, *New J. Chem.*, 2012, **36**, 554-557.
16 (a) P. Thuéry and B. Masci, *Cryst. Growth Des.*, 2008, **8**, 3430-3436; (b) S. Mistri, E. Zangrando and S. Ch. Manna, *Polyhedron*, 2013, **49**, 252–258; (c) A. Chanthapally, H. S. Quah and J. J. Vittal, *Cryst. Growth Des.,* 2014, **14**, 2605−2613; (d) K.-Y. Choi, I.-T. Lim, *J. Inorg. Organomet. Polym. Mater.*, 2012, **22**, 1194-1199; (e) P. Thuéry, *Eur. J. Inorg. Chem.*, 2013, 4563–4573; (f) P. Thuéry, *Cryst. Eng. Comm.*, 2014, **16**, 1724–1734; (g) Z. Hulvey and A. K. Cheetham. *Solid State Sci.*, 2007, **9**, 137-143; (h) J. Luo, F. Jiang, R. Wang and M. Hong, Jiang, *Inorg. Chem. Commun.*, 2004, **7**, 638–642; (i) P. Díaz-Gallifa, O. Fabelo, J. Pasan, L. Canadillas-Delgado, J. Rodríguez-Carvajal, F. Lloret, M. Julve and C. Ruiz-Pérez, *Inorg. Chem.*, 2014, **53**, 5674-5683; (i) Y. Kim and D.-Y., Jung, *Inorg. Chim. Acta*, 2002, **338**, 229-234; (k) M. Menelaou, N. Lalioti, V. Psycharis, C. P. Raptopoulou, A. Terzis, C. Mateescu and A. Salifoglou, *Polyhedron*, 2012, **40**, 134–144.
17 J.-J. Jiang, J.-R. He, X.-Q. Lü, D.-W. Wang, G.-B. Li and Ch.-Y. Su, *IUCrJ*, 2014, **1**, 318–327.
18 L. Palatinus and G. Chapuis, *J. Appl. Cryst*., 2007, **40**, 786–790.
19 G. M. Sheldrick, *Acta Cryst. A*, 2008, **64**, 112–122.
20 C. B. Hübschle, G. M. Sheldrick and B. Dittrich, *J. Appl. Cryst.*, 2011, **44**, 1281–1284.
21 A. L., Spek, *Acta Cryst. C*, 2014, **71**, 9–18.
22 A. L. Spek, *J. Appl. Cryst.*, 2003, **36**, 7–13.
23 H. Putz, MATCH2!, Version 2.2.3., 2014, Crystal Impact GbR, Bonn, Germany.
24 (a) G. Kresse, and J. Hafner, *Phys. Rev. B*, 1993, **47**, 558-561; (b) G. Kresse, and J. Furthmüller, *Phys. Rev. B*, 1996, **54**, 11169-11186.
25 J. P. Perdew, and Y. Wang, *Phys. Rev. B*, 1992, **45**, 13244-13249.
26 P. Blöchl, *Phys. Rev. B*, 1994, **50**, 17953-17979.
27 G. Kresse and D. Joubert, *Phys. Rev. B*, 1999, **59**, 1758-1774.
28 H. Monkhorst and J. Pack, *Phys. Rev. B*, 1976, **13**, 5188-5192.
29 (a) T. Watanabe, S. Keskin, S. Nair and D. S. Sholl, Phys. *Chem. Chem. Phys.*, 2009, **11**, 11389-11394; (b) F. M. Mulder, T. J. Dingemans, M. Wagemaker and G. J. Kearley, *Chem. Phys.*, 2005, **317**, 113-118; (c) L.-M. Yang, P. Ravindran, P. Vajeeston, S. Svelle and M. Tilset, *Micropor. Mesopor. Mat.*, 2013, **175**, 50–58.
30 (a) A. Briceño, D. Leal and G. Díaz de Delgado, *New J. Chem.*, 2015, DOI: 10.1039/C5NJ00678C; (b) A. M. P. Peedikakkal, C. S. Y. Peh, L. L. Koh and J. J. Vittal*, Inorg. Chem.*, 2010, **49**, 6775−6777; (c) G. K. Kole, L. L. Koh, S. Y. Lee, S. S. Lee and J. J. Vittal, *Chem. Commun.*, 2010, **46**, 3660–3662.
31 (a) V. A. Blatov, A. P. Shevchenko, D. M. Proserpio, *Cryst. Growth Des.*, 2014, **14**, 3576-3586; (b) www.topos.ssu.samara.ru.
32 (a) I. D. Brown, *Chem. Rev.*, 2009, **109**, 6858–6919; (b) I. D. Brown, *Struct. Bond.*, 2014, **158**, 11–58.
33 D. Cremer & J. A. Pople, *J. Amer. Chem. Soc.*, 1975, **97**, 1354-1358.
34 J. C. MacDonald, P. C. Dorrestein and M. M. Pilley, *Cryst. Growth Des.*, 2001, **1**, 29-38.
35 S. Ide, N. Karacan and Y. Tufan, *Acta Crystallogr. C*, 1995, **51**, 2304-2305.
36 I. J. Bruno, J. C. Cole, M. Kessler, J. Luo, W. D. S Motherwell, L. H. Purkis, B. R. Smith, R. Taylor, R. I. Copper, S. E. Harris and A. G. Orpen, *J. Chem. Inf. Comput. Sci.*, 2004, **44**, 2133-2144.
37 F. H. Allen, *Acta Cryst. B*, 2002, **58**, 380-388.
38 (a) C. F. Macrae, I. J. Bruno, J. A. Chisholm, P. R. Edgington, P. McCabe, E. Pidcock, L. Rodriguez-Monge, R. Taylor, J. van de Streek and P. A. Wood*, J. Appl. Cryst.*, 2008, **41**, 466-470; (b) Mercury CSD 3.3 (Build RC5), Created on mar oct 15 17:04:41 2013, Copyright CCDC 2001-2013.
39 J.-P. Zhang, X-C Huang, and X.-M. Chenm, *Chem. Soc. Rev.*, 2009, **38**, 2385–2396.
40 R. M. Barrer, Hydrothermal Chemistry of Zeolites, Academic Press, New York, 1982.
41 (a) J. Martí-Rujas and M. Kawano, *Acc. Chem. Res.*, 2013, **46**, 493-505; (b) J. Martí-Rujas, N. Islam, D. Hashizume, F. Izumi, M. Fujita and M. Kawano*, J. Am. Chem. Soc.*, 2011, **133**, 5853–5860; (c) F. C. Pigge, *Cryst. Eng. Comm.*, 2011, **13**, 1733-1748; (d) L. Carlucci, G. Ciani, J. M. García-Ruiz, M. Moret, D. M. Proserpio and S. Rizzato, *Cryst. Growth & Des.*, 2009, **9**, 5024-5034; (e) M. C. Bernini, V. A. de la Peña-O'Shea, M. Iglesias, N. Snejko, E. Gutierrez-Puebla, E. V. Brusau, G. E. Narda, F. Illas and M. A. Monge, *Inorg. Chem.*, 2010, **49**, 5063–5071; (f) Y.-X. Sun and W.-Y. Sun, *Chin. Chem. Lett.*, 2015, **25**, 823–828.
42 (a) J. A. Kaduk, *Powder Diffr.*, 2007, **22**, 74-82; (b) J. A. Kaduk, *Powder Diffr.*, 2007, **22**, 268-278.
43 T. Steiner, *Angew. Chem. Int. Ed.*, 2002, **41**, 48-76.

Graphical Abstract

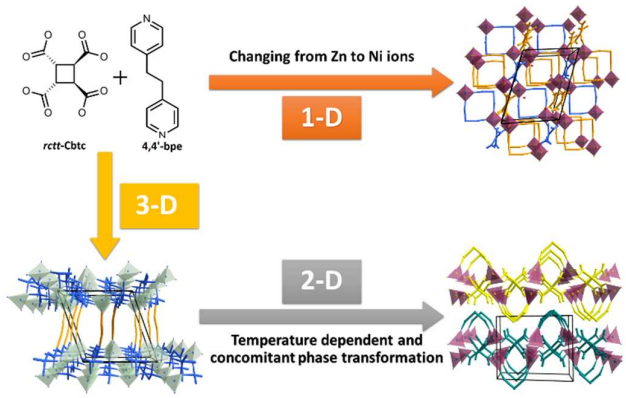

Three novel coordination polymers based on the combination of *rctt*-1,2,3,4-cyclobutanetretracarboxylic acid (*rctt*-H_4Cbtc) and *trans*-1,2-bis(4-pyridyl)ethane (4,4'-bpe) with Zn and Ni metal nodes have been hydrothermally synthesized. Where two of these compounds are an unusual example for the preparation of metastable phase's involving temperature dependent and concomitant transformation.